Springer

Journal of Mechanical Science and Technology 23 (2009) 659~666

Journal of Mechanical Science and Technology

www.springerlink.com/content/1738-494x
DOI 10.1007/s12206-008-1222-y

Numerical evaluation of NO_x mechanisms in methane-air counterflow premixed flames †

Eun-Seong Cho[1] and Suk Ho Chung[2,*]

[1]*Process and Energy, Delft University of Technology, 2628 CA Delft, The Netherlands*
[2]*School of Mechanical and Aerospace Engineering, Seoul National University, Seoul 151-744, Korea*

(Manuscript Received May 13, 2008; Revised August 12, 2008; Accepted December 24, 2008)

Abstract

The control of nitrogen oxides (NO_x) has been a major issue in designing combustion systems, since NO_x play a key role in ozone depletion and the generation of photochemical smog. The characteristics of NO_x emission can be essential information for the development of a clean combustor having suitable reduction methodologies. In the present study, NO_x emission characteristics were evaluated numerically, accounting for the effect of equivalence ratio, stretch rate, pressure, and initial temperature. In general, peak NO_x emission appeared near the equivalence ratio of unity case, and NO_x emission increased with pressure and initial temperature due to the temperature sensitivity in NO_x mechanism. NO_x decreased with stretch rate due to the decrease in residence time in high temperature region. Furthermore, the thermal and prompt mechanisms were evaluated with equivalence ratio for two calculation methods. The conventional methods ignore the interaction of coupled mechanism of thermal and prompt NO_x. The reaction path diagram was introduced to understand effective reaction pathways in various conditions.

Keywords: CHEMKIN; Counterflow premixed flame; Thermal NO_x; Prompt NO_x

1. Introduction

Increased utilization of fossil fuels has led to a rapid increase in the global levels of air pollution such as oxides of nitrogen (NO_x), sulfur (SO_x), carbon (CO_x), unburned and partially burned hydrocarbons (UHC), and particulate matter [1, 2]. Air pollutants have detrimental effects on the environment and human health in a number of ways. Hence, the control of pollutant emissions has become an essential factor in the design of modern combustion systems. Legislations and regulations on air quality standards have been enforced so there is an urgency to develop low emission combustion system.

Nitrogen oxide is one of the major pollutants of fossil fuel combustion, and the recent concern of environmental protection has resulted in increasingly stringent NO_x emission regulations in a number of industrialized countries [3]. There is an urgent need to develop low emission combustion devices. Our fundamental knowledge of the combustion reaction of hydrocarbon fuels and the reaction mechanisms leading to NO_x formation is now at a certain level [4]. However, the complicated interacting processes between flow and chemistry make it difficult to understand NO_x formation process in flames. A typical example is turbulent flames, which are most frequently used in practical combustion devices. Even in the laminar flames, which are commonly used in small gas appliances, the flow is multi-dimensional, and it is still difficult to study experimentally the formation process in the flames. On the other hand, numerical calculation required to describe the flow and the chemistry of the detailed mechanisms, would

† This paper was recommended for publication in revised form by Associate Editor Kyoung Doug Min

*Corresponding author. Tel.: +82 2 880 7114, Fax.: +82 2 889 1842
E-mail address: shchung@snu.ac.kr

become too large to be handled even by supercomputers. However, we have to find the way to study the NO_x emission characteristics in flames and further to understand the formation processes so as to develop low emission devices.

The first step is to study the emission characteristics in fundamental premixed flames of simple laminar flows and for methane fuel, which is the simplest hydrocarbon fuel. To understand the emission behavior, a numerical approach can be the appropriate one, if detailed kinetic mechanisms can be implemented. If the calculation is accurate enough to reproduce the essential features, one can use the result to find the underlying physics and chemistry by investigating the interaction between chemistry and transport processes. The respective elementary reactions in the reaction mechanism are closely related to transport processes, and hence the roles played by the respective reactions leading to NO_x formation. They will also depend on flame parameters, such as equivalence ratio and stretch rate. One can elucidate this process through numerical calculations to understand the different emission behavior.

The flow field of premixed flame is usually multi-dimensional. However, the recent experimental studies have shown that fundamental flame properties of these flames can be studied by using a counterflow as a model [5-7]. The actual flow field in this counterflow is two-dimensional, yet the flame remains planar. Thus, one can use the similarity solutions to reduce the governing equations to ordinary differential equations.

2. Governing equations and numerical analysis

CHEMKIN III [8] based OPPDIF [9] code can compute steady-state solutions for axisymmetric flames. The quasi-one-dimensional model can predict the species, temperature, and velocity profiles in the core flow between the nozzles (excluding edge effects).

The counterflow geometry is well known, which consists of two concentric, circular nozzles directed towards each other. This configuration produces an axisymmetric flow field with a stagnation plane between the nozzles. The location of the stagnation plane depends on the momentum balance of the two streams. When the streams are premixed, two premixed flames exist, one on either side of the stagnation plane.

The opposed-flow geometry makes an attractive experimental configuration, because the flames are flat, allowing for detailed study of the flame chemistry and structure. The two-dimensional flow is reduced to quasi-one-dimension by assuming that the radial velocity varies linearly in the radial direction, which leads to a simplification in which the fluid properties are functions of the axial distance only.

The reduction of the two-dimensional stagnation flow is based on similarity solutions advanced in incompressible flows by von Kármán, which are available in Schlichting [10].

A derivation of the governing equations for the opposed-flow geometry is given in brief.

At steady-state, conservation of mass in cylindrical coordinates is

$$\frac{\partial}{\partial x}(\rho u)+\frac{1}{r}\frac{\partial}{\partial r}(\rho v r)=0 \tag{1}$$

where, x, r and u, v are axial and radial directions and velocity components, respectively, and ρ is the density. Following von Kármán, who recognized that v/r and other variables should be functions of x only,

$$G(x)=-\frac{\rho v}{r} \quad \text{and} \quad F(x)=\frac{\rho u}{2} \tag{2}$$

for which the continuity equation reduces to

$$G(x)=\frac{dF(x)}{dx} \tag{3}$$

for the axial velocity u. Since F and G are functions of x only, so are ρ, u, T, and Y_k.

$$H=\frac{1}{r}\frac{\partial p}{\partial r}=\text{constant} \tag{4}$$

where p is the pressure.

The radial momentum equation becomes

$$H-2\frac{d}{dx}\left(\frac{FG}{\rho}\right)+\frac{3G^2}{\rho}+\frac{d}{dx}\left[\mu\frac{d}{dx}\left(\frac{G}{\rho}\right)\right]=0 \tag{5}$$

Energy and species conservation are

$$\rho u\frac{dT}{dx}-\frac{1}{c_p}\frac{d}{dx}\left(\lambda\frac{dT}{dx}\right)+\frac{\rho}{c_p}\sum_k c_{pk}Y_k V_k\frac{dT}{dx} \tag{6}$$

$$+\frac{1}{c_p}\sum_k h_k\dot{\omega}_k = 0$$

where T is the temperature; $Y_k, W_k, \dot{\omega}_k, c_{pk}$, and h_k are the mass fraction, the molecular weight, the reaction rate, the specific heat, and the enthalpy of kth species, respectively; c_p is the mixture specific heat and λ and μ are the thermal conductivity and the viscosity, respectively.

The diffusion velocities are given by either the multi-component formulation

$$\rho u\frac{dY_k}{dx}+\frac{d}{dx}(\rho Y_k V_k)-\dot{\omega}_k W_k = 0 \qquad k=1,\ K \tag{7}$$

or the mixture-averaged formulation

$$V_k = \frac{1}{X_k\bar{W}}\sum_{j=1}^{K} W_j D_{kj}\frac{dX_j}{dx}-\frac{D_k^T}{\rho Y_k}\frac{1}{T}\frac{dT}{dx} \tag{8}$$

$$V_k = -\frac{1}{X_k}D_{km}\frac{dX_k}{dx}-\frac{D_k^T}{\rho Y_k}\frac{1}{T}\frac{dT}{dx}$$
$$where,\ D_{km}=\frac{1-Y_k}{\sum_{j\neq k}^{K} X_j/D_{jk}} \tag{9}$$

where X_k and $\bar{W}$ are mole fraction and the average molecular weight, respectively; D_{kj}, D_{km}, D_{jk} and D^T_k are the multi-component, mixture averaged, binary, and thermal diffusion coefficients, respectively.

The boundary conditions for the lower (*1*) and upper (*2*) streams at the nozzles are

$$x=0:\ F=\frac{\rho_1 u_1}{2},\ G=0,\ T=T_1,\ \rho u Y_k+\rho Y_k V_k=(\rho u Y_k)_1$$
$$x=X:\ F=\frac{\rho_2 u_2}{2},\ G=0,\ T=T_2,\ \rho u Y_k+\rho Y_k V_k=(\rho u Y_k)_2 \tag{10}$$

3. NO_x mechanisms

The adopted reaction scheme to describe combustion reactions in the flames was the GRI 3.0 mechanism [11] where there are 40 NO related reactions. In describing NO formation, prompt and thermal mechanisms were used. The former includes the mechanism through N_2O, in addition to Fenimore mechanism. The reactions leading to NO_2 formation are also included [6].

The contribution of the respective NO formation mechanism in total NO production was evaluated in the following way, where the numbers in parenthesis correspond to that in the GRI 3.0 mechanism [11].

a) Thermal NO (Zeldovich) is the one obtained by the following three mechanisms.

$$\begin{array}{ll} O + N_2 \leftrightarrow NO + N & (\text{-R178}) \\ N + O_2 \leftrightarrow NO + O & (\text{R179}) \\ N + OH \leftrightarrow NO + H & (\text{R180}) \end{array} \tag{11}$$

b) N_2O mechanism is the summation of production through the following three reactions in the full mechanism calculation.

$$\begin{array}{ll} N_2O + O \leftrightarrow 2NO & (\text{R182}) \\ N_2O + H \leftrightarrow NH + NO & (\text{R199}) \\ N_2O + CO \leftrightarrow NCO + NO & (\text{-R228}) \end{array} \tag{12}$$

c) NO_2 mechanism is the summation of production through the following five reactions in the full mechanism calculation.

$$\begin{array}{ll} NO_2 + OH \leftrightarrow HO_2 + NO & (\text{-R186}) \\ NO_2 + M \leftrightarrow O + M + NO & (\text{-R187}) \\ NO_2 + O \leftrightarrow O_2 + NO & (\text{R188}) \\ NO_2 + H \leftrightarrow OH + NO & (\text{R189}) \\ NO_2 + CN \leftrightarrow NCO + NO & (\text{R281}) \end{array} \tag{13}$$

d) Prompt NO (Fenimore) mechanism is the one obtained by the full mechanism calculation minus the summation of the above three mechanisms.

Using these classifications the portion of each mechanism can be evaluated in the numerical calculation. This is one advantage of numerical study over experimental study because the experimental result only showed global NO emission.

In the conventional method [6], calculations had to be done two times in the same condition. One was thermal NO emission, which was calculated by using hydrocarbon chemistry and the thermal mechanism (reactions (*R178*)-(*R180*)), and the other was full chemistry calculation. Prompt NO was obtained by subtracting the amount of NO calculated by thermal mechanism from the results of the full chemistry. However, the thermal and prompt mechanisms are strongly coupled so the role of the thermal mechanism in the full chemistry may be very different from that in the case of C_3 chemistry and the thermal

mechanism alone [12]. These differences will be discussed later.

In this study, the calculation had to be done only one time using full chemistry and then using the post-processing program to sort the production of each mechanism.

4. Results and discussion

4.1 Characteristics of NO production

NO emission characteristics of premixed flames were evaluated at various conditions at especially high temperature and high pressure conditions because numerical calculation could easily obtain the results even though they can be difficult to realize experimentally.

The fuel used was methane (CH_4), which is the main component of natural gas. The calculation variables are stretch rate, equivalence ratio, pressure, and initial temperature.

(1) Stretch rate effect

The stretch rate was calculated from the velocity and density of each side of nozzle condition [13] as follows:

$$\kappa = 2\frac{-u_1}{L}\left[1+\frac{u_2}{-u_1}\sqrt{\frac{\rho_2}{\rho_1}}\right] \tag{14}$$

u is the velocity of each nozzle and ρ is density. Subscripts *1* and *2* indicate each side of nozzle and L means nozzle distance. In this research, both sides of nozzles have the same composition of fuel and air mixture and exit velocity. The distance of each nozzle (L) is 2 cm.

The characteristics of NO production can be represented by the emission index of NO (EINO) following the procedure of Takeno and Nishioka [14], which is defined in terms of the NO production rate, $\dot{\omega}_{NO}$, and the fuel consumption rate, $-\dot{\omega}_F$ as shown in Eq. (5):

$$EINO = \frac{\int_{-L}^{L}\dot{\omega}_{NO}W_{NO}dx}{-\int_{-L}^{L}\dot{\omega}_{F}W_{F}dx} \tag{15}$$

where W_{NO} and W_F are the molecular weights of nitric oxide and fuel, respectively.

Fig. 1 shows the EINO and EINO percentage depending on the formation mechanisms with stretch rate at temperature of 300 K and at the ambient pressure of 1 atm with the equivalence ratio ϕ of 1.0. The total EINO decreases with stretch rate because high flow velocity reduces the residence time in the high temperature region and the temperature decreased with stretch rate. The percentage of thermal NO mechanism decreased and then increased with stretch rate, but the trend of prompt NO is the reverse. The contributions from N_2O and NO_2 mechanisms were nearly zero.

(2) Equivalence ratio effects

Fig. 2 shows the EINO and EINO percentage with equivalence ratio in high temperature (800 K) and ambient pressure condition and the stretch rate of κ =1000 s^{-1}. The maximum NO emission showed at near the stoichiometric condition and decreased in

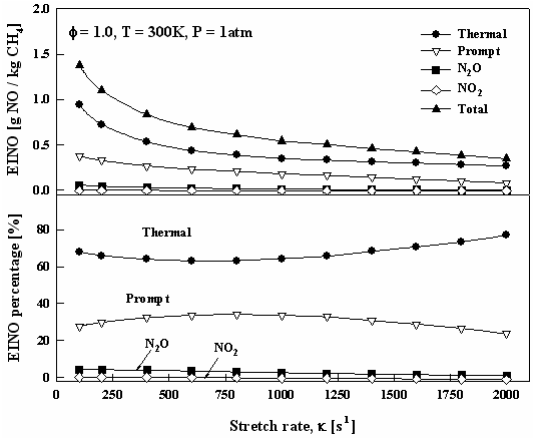

Fig. 1. EINO with stretch rate for each NO mechanism.

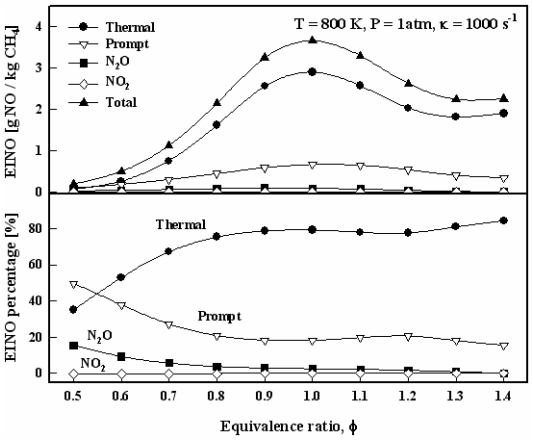

Fig. 2. EINO with equivalence ratio for each NO mechanism.

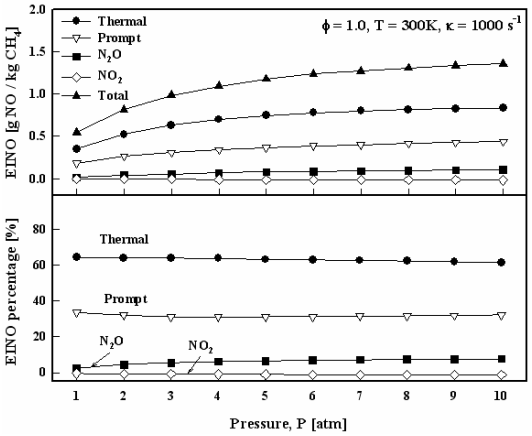

Fig. 3. EINO with pressure for each NO mechanism.

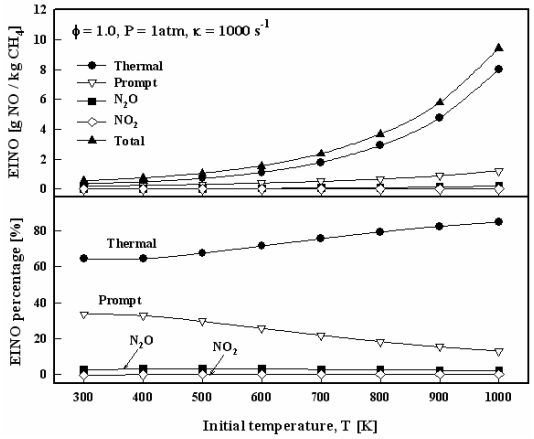

Fig. 4. EINO with initial temperature for each NO mechanism.

rich and lean sides. The thermal mechanism increased with equivalence ratio and prompt decreased until ϕ =1.0 and increased with ϕ in rich conditions. Previously [6], it was found that the rich condition predominantly existed with prompt NO emission, but the present result does not agree with the previous one [6]. This reason will be discussed later. The contribution from N_2O mechanism decreased with equivalence ratio increase, but NO_2 mechanisms were not changed regardless of equivalence ratio and nearly zero.

(3) Pressure effect

Fig. 3 shows the EINO and EINO percentage with pressure in temperature of 300 K with ϕ =1.0 and κ =1000 s^{-1}. The EINO gradually increased with pressure because temperature increased with pressure,

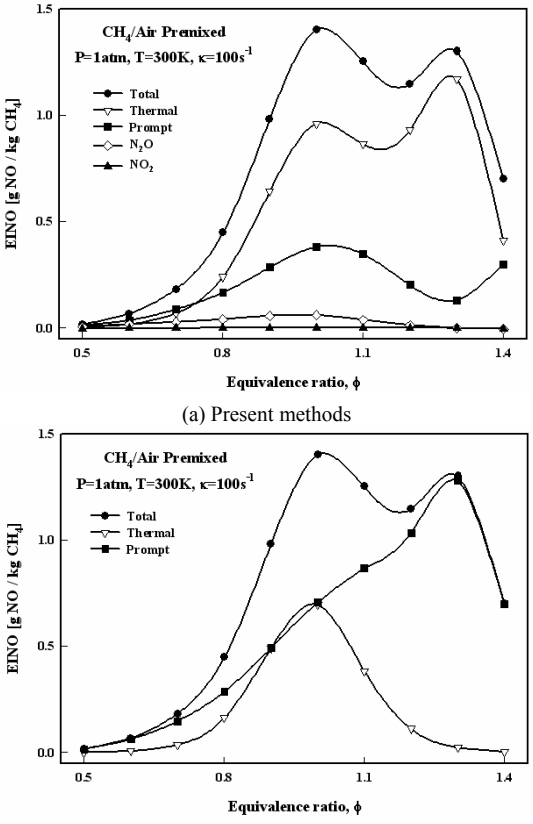

Fig. 5. EINO calculated by present and conventional methods with equivalence ratio.

even though it is not shown here. The EINO percentage of all mechanisms was not much varied with pressure.

(4) Initial temperature effect

Fig. 4 shows EINO and EINO percentage with initial temperature at ambient pressure with ϕ =1.0 and κ =1000 s^{-1}. The NO emission rapidly increased with initial temperature, which showed the NO characteristics to be strongly dependent on temperature. Percentage of thermal EINO increased with temperature but prompt NO decreased.

4.2 Evaluation of thermal and prompt NO formation characteristics

As mentioned above, the prompt NO was calculated by the extraction of the contribution of thermal NO chemistry from that of full chemistry results in the conventional method [6]. In the present study, the

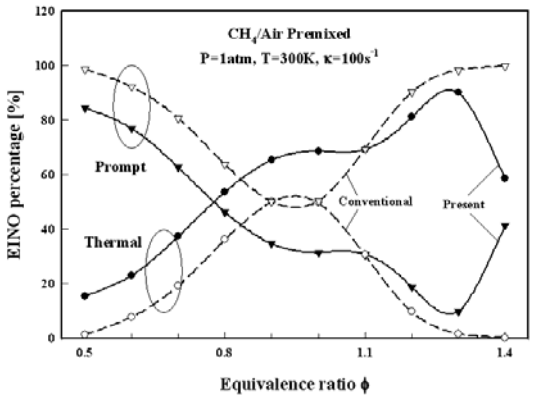

Fig. 6. Thermal and prompt EINO percentage with equivalence ratio compared with present and conventional methods.

post processing program could extract the contribution of each mechanism of EINO from the full chemistry results. These two results were different, especially rich equivalence ratio conditions

Fig. 5 shows the EINO for each mechanism with equivalence ratio for the present and conventional methods. For the present method, the predominant NO production is the thermal mechanism for almost all equivalence ratios. But the conventional method showed that the prompt NO mechanism was dominant in fuel rich condition ($\phi \geq 1.0$).

Each prompt and thermal NO percentage is shown in Fig. 6. Up to $\phi = 1.0$, both methods have similar trends, that is, the thermal NO increases and the prompt NO decreases with equivalence ratio even though the percentages are somewhat different. For the equivalence ratio larger than 1.0, the two mechanisms have extraordinarily different trends. The prompt NO increased with equivalence ratio in the conventional method, while the present method showed that the prompt NO gradually decreased with equivalence ratio until $\phi = 1.3$.

To evaluate the difference of the two methods, the thermal NO production rate is illustrated in Fig. 7.

The conventional method showed only the thermal NO mechanism and the present method calculated with the full chemistry and extracted the thermal mechanism using post processing program. The thermal NO mechanism consisted of three reaction steps: N and NO production step of $N_2+O \rightarrow N+NO$ (*-R178*) and N consumption and NO production steps of (*R179*) and (*R180*).

The NO production rates by the reaction step of (*-R178*) were similar for the two methods, while those

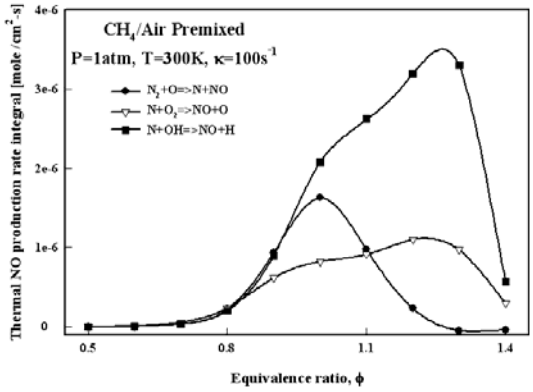

(a) Present method

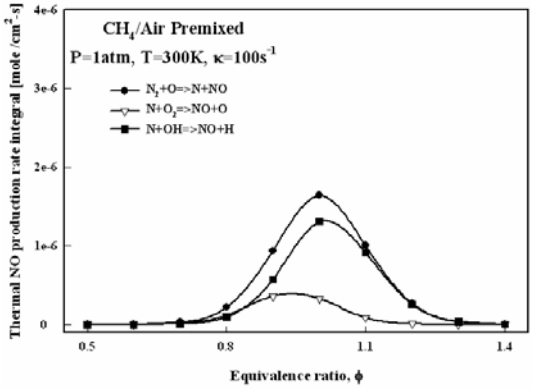

(b) Conventional method

Fig. 7. Thermal NO production rate in present and conventional methods with equivalence ratio.

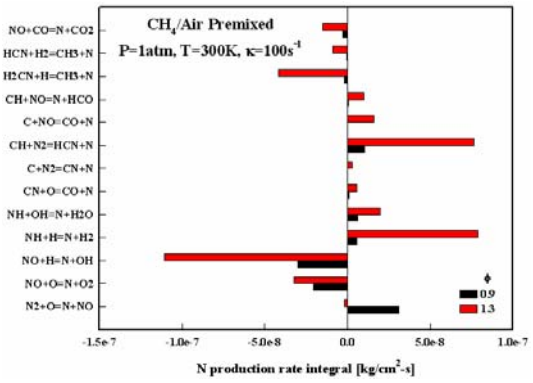

Fig. 8. N production rate integration of reaction steps with equivalence ratio.

for other two reactions were quite different, especially for rich conditions. The reaction steps of (*R179*) and (*R180*) produced EINO using N species via way of (*-R178*) reaction step in when only the thermal

mechanism was considered. But the full chemistry had another source of N species to produce NO emission.

To evaluate the difference, major N production steps are illustrated in Fig. 8. The lean (ϕ =0.9) and rich (ϕ =1.3) cases were compared.

The lean case corresponds to the condition that the conventional and present methods were similar. The calculations were performed with the full chemistry mechanism. Fig. 8 shows that N is predominantly produced by the reaction step of $N_2+O \rightarrow N+NO$ in the lean case. In the rich case, N is produced mainly by two steps of $CH+N_2 \rightarrow HCN+N$ (*R240*) and $NH+H \rightarrow N+H_2$ (*R196*). They supplied N to thermal NO reaction steps of (*R179*) and (*R180*) and produced NO remarkably.

Fig. 9 shows effective NO production steps for ϕ =0.9 and 1.3. In the lean case, NO production by thermal mechanism was appreciably compared with the prompt mechanism. In the rich case, the dominant NO reaction was through the prompt mechanism, especially $HNO+H=H_2+NO$, even though there was a step with negative peak of $HNO+M=H+NO+M$.

The NO emissions were produced through thermal NO and prompt NO mechanism, where the original source of N was the thermal steps for the lean case and the prompt step for the rich case. Note that N species produced from the prompt mechanism could produce NO through the thermal NO mechanism.

To better understand the NO mechanism the reaction path diagram was introduced [12]. Fig. 10 shows the reaction path diagram of the lean and rich conditions. All reaction steps are coupled and interacting so the reaction path diagram could be helpful to understand NO emission characteristics under various conditions.

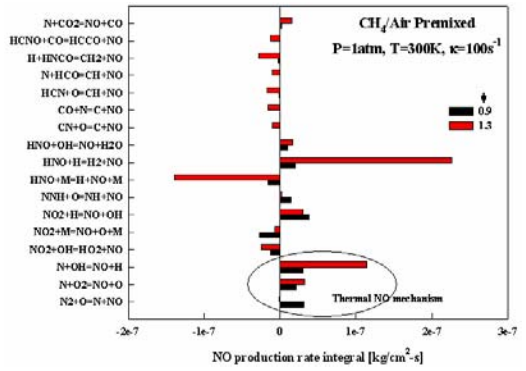

Fig. 9. NO production rate integration of reaction steps with equivalence ratio.

5. Conclusions

The NO emission characteristics were studied numerically for various conditions.

1. EINO decreased with stretch rate because of the short residence time in the high temperature region, which reduced flame temperature.
2. Maximum EINO showed at the equivalence ratio of 1.0 and decreased for lean and rich conditions. This trend was similar to the maximum temperature trend with equivalence ratio, which shows the temperature dependent characteristics of NO emission.
3. EINO rapidly increased with initial temperature in premixed condition. EINO also increased with pressure, especially at high temperature conditions. High temperature together with high pressure condition must be considered carefully in reducing NO emission.
4. The thermal and prompt mechanisms were

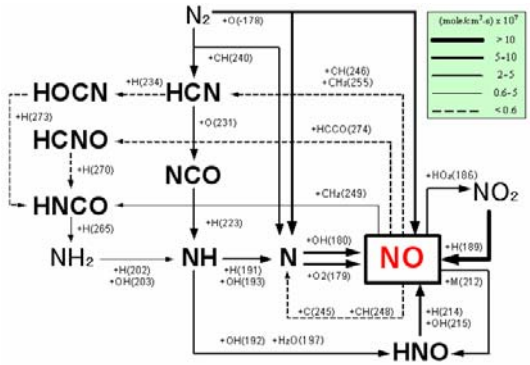

(a) Equivalence ratio (ϕ =0.9)

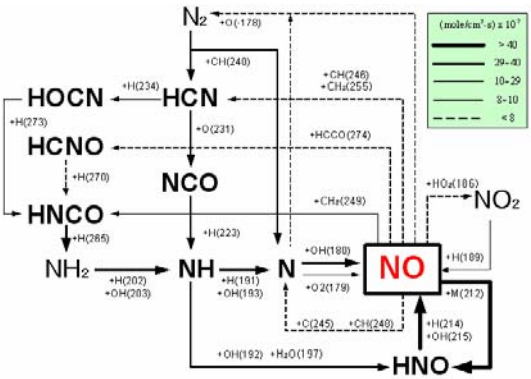

(b) Equivalence ratio (ϕ =1.3)

Fig. 10. NO reaction path for lean (ϕ =0.9) and rich (ϕ =1.3) cases.

evaluated with equivalence ratio for two calcula tion methods. The results of each method have a different trend, especially in fuel rich condition, because the conventional methods ignore the interaction of the coupled mechanism of thermal and prompt NO. A reaction path diagram was introduced to understand the effective reaction pathways in various conditions.

Acknowledgment

This work was supported by Oxy-PC Project from KITECH through IAMD.

References

[1] A. H. Lefebvre, *Gas Turbine Combustion,* Taylor & Francis, (1983).

[2] A. M. Mellor, Gas Turbine Engine Pollution, *Prog. Energy Combust. Sci*. 1 (1976) 111-133.

[3] C. T. Bowman, Control of Combustion Generated Nitrogen Oxide Emissions: Technology Driven by Regulation, *Proc. Combust. Instit.* 24 (1992) 859-878.

[4] J. A. Miller and C. T. Bowman, Mechanism and Modeling of Nitrogen Chemistry in Combustion, *Prog. Energy Combust. Sci*. 15 (1989) 287-338.

[5] H. Tsuji, Counterflow Diffusion Flames, *Prog. Energy Combust. Sci*. 8 (1982) 93-119.

[6] M. Nishioka et al., NO Emission Characteristics of Methane-Air Double Flame, *Combust. Flame* 98 (1994) 127-138.

[7] E.-S. Cho and S. H. Chung, Numerical Study on NO Emission with Flue Gas Dilution in Air and Fuel Sides, *J. of Mech. Sci. Technol.* (*KSME Int'l J.)* 19 (2005) 1393-1400.

[8] R. J. Kee et al., CHEMKIN-III: A FORTRAN Chemical Kinetics Package for the Analysis of Gas-Phase Chemical and Plasma Kinetics. Sandia National Laboratories Report, *SAND 96-8216* (1996).

[9] A. E. Lutz et al., OPPDIF: A FORTRAN Program for Computing Opposed-Flow Diffusion Flames, Sandia National Laboratories Report, *SAND96-8243* (1997).

[10] H. Schlichting and K. Gersten, *Boundary Layer Theory,* 8th Revised and Enlarged Edition, Springer-Verlag, New York (2000).

[11] G. P. Smith et al., Gri-Mech 3.0. http://www.me. berkeley.edu/ gri_mech/ (2000).

[12] Y. Ju and T. Niioka, Computation of NO_x Emission of a Methane-Air Diffusion Flame in a Two-Dimensional Laminar Jet with Detailed Chemistry, *Combust. Theory Modeling* 1 (1997) 243-258.

[13] H. K. Chellian et al., An Experimental and Theoretical Investigation of the Dilution, Pressure and Flow-Field Effects on the Extinction Condition of Methane-Air-Nitrogen Diffusion Flames, *Proc. Combust. Instit.* 23 (1993) 503-511.

[14] T. Takeno and M. Nishioka, Species Conservation and Emission Indices for Flame Described by Similarity Solutions, *Combust. Flame* 92 (1993) 465-448.

Dr. Eun-Seong Cho received his B.S. and M.S. degrees in Mechanical Engineering from Hanyang University, Korea, in 1996 and 1998, respectively. He then received his Ph.D. degree from Seoul National University, Korea, in 2005. He was a principal engineer of KD Navien research center and currently a research associate at Delft University of Technology, The Netherlands. His research interests include eco-friendly clean combustion technology, new and renewable energy systems.

Prof. Suk Ho Chung received his B.S. degree from Seoul National University, Korea, in 1976 and Ph.D. degree in Mechanical Engineering from Northwestern University, USA, in 1983. He is a Professor since 1984 in the School of Mechanical and Aerospace Engineering at Seoul National University in Seoul, Korea. His research interests cover combustion fundamentals, pollutant formation, laser diagnostics, and plasma-assisted combustion.